geosciences

MDPI

Article

Cultural Heritage and Rockfalls: Analysis of Multi-Scale Processes Nearby the *Lucus Angitiae* Archaeological Site (Central Italy)

Emiliano Di Luzio *, Luca Schilirò and Iolanda Gaudiosi

CNR-IGAG, Consiglio Nazionale delle Ricerche, Istituto di Geologia Ambientale e Geoingegneria, Montelibretti, Via Salaria km 29.3, Monterotondo St., 00165 Rome, Italy; luca.schiliro@igag.cnr.it (L.S.); iolanda.gaudiosi@igag.cnr.it (I.G.)

* Correspondence: emiliano.diluzio@igag.cnr.it

Abstract: Archaeological areas in the mountain region of central Italy can be seriously threatened by geological hazards, and efforts are required to preserve cultural heritage. The *Lucus Angitiae* is a pre-Roman site located along the western edge of the Fucino Basin, the largest continental depression of central Apennines. The carbonate slope overhanging the area is affected by active rockfall processes from two main rock escarpments. In this paper, rockfall assessment was pursued through a 3D kinematic modelling, performed by adopting a probabilistic approach. Specific attention was dedicated to the choice and calibration of the input data, based on field evidence and a literature review. Two different sizes of wedge-shaped rock blocks were identified on rock escarpments, and specific stability analyses were performed. Sensitivity analyses accounting for possible triggering factors, such as water pressure increase and seismic action, were also carried out, together with an investigation of the seismological characteristics of the area. The results of the numerical simulations were used to design effective countermeasures in the framework of a mitigation plan for protection of the archaeological site. Finally, clues of gravity-driven slope deformations at the slope scale were documented, framing the rockfall process in a wider geological scenario.

Keywords: rockfall; probabilistic modeling; cultural heritage; *Lucus Angitiae*; central Italy

Citation: Di Luzio, E.; Schilirò, L.; Gaudiosi, I. Cultural Heritage and Rockfalls: Analysis of Multi-Scale Processes Nearby the *Lucus Angitiae* Archaeological Site (Central Italy). *Geosciences* **2021**, *11*, 521. https://doi.org/10.3390/geosciences11120521

Academic Editors: Deodato Tapete and Jesus Martinez-Frias

Received: 29 September 2021
Accepted: 10 December 2021
Published: 17 December 2021

1. Introduction

Natural hazards, such as earthquakes, volcanic eruptions, and tsunamis, represent a major concern for the safety and development of human society but, at the same time, pose a serious threat to the conservation of tangible cultural heritage across the world [1]. Even landslides may represent a hazardous phenomenon, since they can damage access roads and tourist paths to cultural heritage sites as recently observed, for instance, in the Machu Picchu archeological site [2] or the Cinque Terre area [3]. In other cases, landslides can directly threaten the integrity of sites located in mountainous regions and relatively high relief areas [4–7]. For this reason, many efforts are being made for developing interdisciplinary approaches devoted to the assessment of landslide hazard in such areas [8–10], also through new technologies such as remote sensing techniques [11–14], with the aim of improving specific management plans [15–17]. In this work we analyzed active rockfall processes threatening the *Lucus Angitiae* archaeological site, which is located north of Luco dei Marsi, a small village in the Apennine region of central Italy (Figure 1). The archaeological area retains traces of prehistoric huts and graves dating back to the X century BCE (i.e., Before Common Era), but also remnants of pre-roman fortified walls, terraces, and tanks. Indeed, before the Roman occupation (since the IV century BCE), an important sanctuary dedicated to goddess Angitia was constructed in this place by the *Marsi*, an ancient Italic population. According to the mythological tradition, Angitia ruled healing and witchcraft and she has been identified with Greek Medea [18].

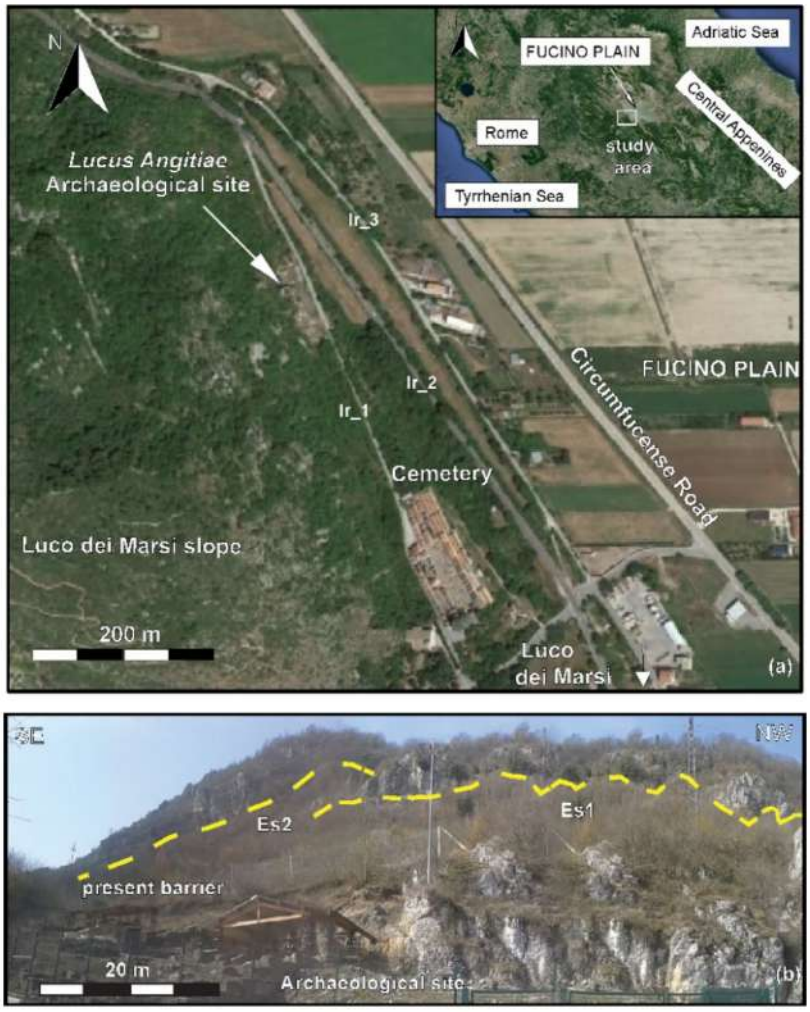

Figure 1. (**a**) Aerial view of the study area along the western border of the Fucino Basin in central Italy (see the upper right insight). The position of the *Lucus Angitiae* archaeological site and the local road network (Circumfucense Road and lr_1-3) is also reported; (**b**) rock slope escarpments Es1 and Es2 impending on the archaeological site. It is worth noting the presence of elastic barriers which partially protect the site.

The rockfall activity is testified by tens of fallen rock blocks found along the piedmont junction zone and into the archaeological area (Figure 2a–e). A rockfall event occurred in December 2005 was reported by local newspapers (Figure 2f) and caused serious damage to the archaeological site, including the collapse of protective roofs [19]. Due to the lack of other historical records, the main aim of this work is limited to a rockfall susceptibility assessment. This goal was pursued through the Rotomap® software code [20,21], a physically-based, spatially-distributed probabilistic model, which adopts a lumped-mass approach [6,7,22–24]. The code performs a 3D probabilistic simulation considering the lateral dispersion effects along slopes (unlike a 2D model). In this way, it was possible to reconstruct: (i) possible rockfall trajectories; (ii) run-out distances; (iii) spatial distribution of endpoints; (iv) spatial variations of specific kinetic energy and trajectory height for dimensionless rock blocks.

Different volumes of design blocks were recognized by analyzing the size of the inventoried fallen boulders and the characteristics of joints on rock escarpments. The results of numerical simulations were used for drafting a mitigation plan which includes efficacy evaluation of pre-existing retaining structures (Figures 1b and 2b) and the design of new elastic barriers.

Figure 2. Example of calcareous rock blocks which can be observed in different parts of the study area. Specifically: (**a**,**b**) within the archaeological site; (**c**) along road lr_3; (**d**) in the middle sector of the slope, blocked by a tree; and (**e**) nearby a wall along the lr_1 roadside; (**f**) local newspaper reporting information about the rockfall event occurred in December 2005.

Geomechanical analyses highlighted two potential examples of rock wedge failures, which may involve rock mass volumes varying from few to hundreds of cubic meters. In both cases, the sensitivity of slope stability conditions to possible triggering mechanisms, such as water pressure within cracks and seismic inputs has been investigated. In the last case, input data were derived from a probabilistic analysis of seismic action.

Alongside these analyses, evidence of wide-open trenches on the eastern edge of the mountain ridge are reported, allowing to infer that rockfall events can be considered as secondary effects of gravity-driven slope deformations.

2. Geological and Geomorphological Setting

The *Lucus Angitiae* archaeological site is located along the western edge of the Fucino Basin, the widest intermontane basin of the central Apennine belt (e.g., [25,26]). The basin formed as a consequence of Late Pliocene-Quaternary normal faulting, which mainly occurred on the northern and eastern margins [27–30]. Due to its tectonic setting, the area is seismically active as testified by numerous historical earthquake events, such as the one occurred in 1915 with Mw > 7 and I_{MCS} > 6 [31–34].

The western edge of the continental depression is bordered by a mountain ridge made up of Upper Cretaceous, shallow water, biodetritic limestone, and dolomitic limestone (UCl in Figure 3a). Dip direction of bedding is towards E and NE, with dipping angles ranging between 20° and 35° in the inner zones of the ridge and between 5° and 15° towards the slope edge (Figure 3b,c). Here, few outcrops of Middle Miocene bioclastic limestone (MMbl) are separated from the underlying Upper Cretaceous limestone by a paraconformity surface (Figure 3d). Finally, the local Quaternary sequence includes the alluvial deposits of the Fucino Basin interfingered with talus slope and debris fan deposits in the piedmont junction zone (Figure 3a).

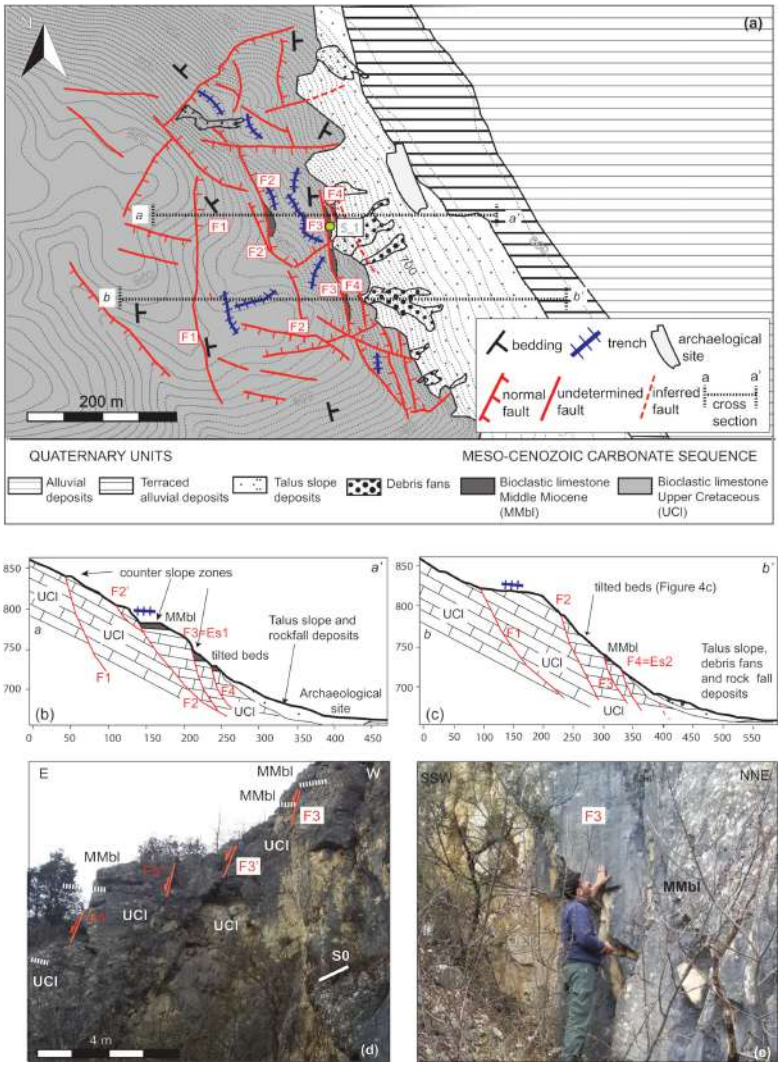

Figure 3. (**a**) Geological map of the study area. Legend: S_1 = geomechanical analysis site; F1-F4 = faults intersecting trace of sections a-a' and b-b'; (**b**), (**c**) geological sections); (**d**) slope-parallel faults (F3-F4 and secondary splays), UCl = Upper Cretaceous limestone; MMb = Middle Miocene bioclastic limestone; (**e**) particular of fault F3.

Normal faults, NNW-SSE trending and mainly ENE-dipping, affect the carbonate sequence nearby the slope edge (Figure 3a–e). Bedding rotation is clear in hanging-wall blocks (Figure 3b,c). Such slope-parallel faults are closely spaced with single vertical displacement in the order of few meters (Figure 3d). These features are dissected by a second system of normal faults striking NE-SW and a third system oriented from E–W to WNW–ESE (Figure 3a), which show a complex kinematics, including strike-slip displacements.

The morphological setting of the slope is highly influenced by the tectonic elements. Two sub-vertical rock escarpments, Es1 and Es2 in Figure 1b, follow the trace of the main NNW-SSE trending normal faults and have an average height of 20 and 10 m, respectively. Slope cliffs are interrupted and separated by wide (up to 15–20 m) trench zones which isolate long (tens of meters) rock slabs (Figure 4a,b). Trenches, slope dip breaks and counter slope sectors (Figure 3b,c), reveal an articulated morphology and, likely, an ongoing gravity-driven deformation.

Figure 4. (**a**,**b**) Panoramic views of the tectonic-controlled escarpments Es1 and Es2 with evidence of main trench zones. The source area of the 2005 rockfall event and first-order rock wedges can be noticed.

3. Materials and Methods

3.1. Rock Blocks Inventory

Evidence of past rockfall events were pointed out through a detailed inventory map including 69 erratic boulders. These blocks are mainly concentrated within the uppermost part of the slope, along a N–S oriented channel at the foot of Es2, and into the archaeological site (Figure 5a), while only a few blocks were observed at mid slope elevations and along the local road networks.

Information regarding location, geometric features, dimensions (length, width, height) and estimated volumes have been stored, for each rock block, in a GIS database. A preliminary statistical analysis (Figure 5b) shows how the block volume ranges between 0.01 and 5.5 m^3, with an average value of 0.66 m^3 and a standard deviation equal to 1.82 m^3. The frequency histogram (Figure 5c) shows a clear bimodal, continuous distribution, with a main and secondary peak in correspondence of 0.25 and 5 m^3, respectively. The few large ($V > 3.0$ m^3) blocks were found only nearby the main escarpments, while the small-volume blocks (generally <1 m^3) were documented in the lower slope sectors only (Figure 5a).

3.2. Rockfall Probabilistic Modeling: Input Data

Several controlling factors can influence the down-slope propagation of rock blocks and a probabilistic approach is needed to simulate phenomena with significant uncertainty. Apart the slope geometry, the RotoMap® code requires as input data few parameters related to the initial motion conditions, such as (i) location of detachment points; (ii) number and values of starting velocities (following the free-fall phase) for each detachment point; (iii) angular deviations from the maximum slope direction. Furthermore, the model calculation is influenced by the spatial distribution along slope of the normal (K_n)/tangential (K_t) elastic restitution coefficients and the dynamic friction angle ($\Phi_{\mu d}$), which control the bouncing and rolling phase of motion, respectively. In this paper, reference values for first step modeling were inferred from a literature review; afterwards, values were calibrated via back-analysis by comparing the numerical results with the inventory map of the rock blocks, whose positions were assumed as endpoints of former rockfall events.

3.2.1. Slope Geometry

A 5 × 5 m cell-size Digital Elevation Model (DEM) was used as input data in the RotoMap® code. From the base of Es1 and Es2, the slope topography shows a biplanar geometry and can be simplified with a proximal sector, having an average slope angle between 20° and 25°, and a distal zone where the slope progressively decreases up to

5° (Figure 3b,c). According to [35,36], the DEM resolution plays an important role in controlling the simulation of rock blocks trajectories, since a low-resolution DEM would not allow a realistic simulation of the lateral dispersion of falling rock blocks. However, in the case of a simple slope geometry, a 5 × 5 m DEM can be considered suitable for performing 3-D modeling [35].

3.2.2. Initial Motion Conditions

Rockfall simulations with Rotomap® code require a series of input data describing the initial motion conditions of detaching rock blocks. These are considered as infinitely small mass points regardless their three-dimensional aspects (shape, dimensions, orientation). Most of these initial motion parameters can be evaluated from the geometric features (i.e., length, height, and dip angle) of the escarpments identified as source areas. In detail, the required parameters are the following:

(a) Number of starting points (nSp): Rotomap® simulates the detachments ì along a starting line corresponding to the base of the cliff, from which the rock blocks move, after the free-fall phase, with an initial velocity V0i $\neq 0$. Since any information was available regarding the location of former rockfall source areas (except for the rock scars of the 2005 event shown in Figure 4a), a conservative approach was adopted, and starting points were placed along the entire length of Es1 and Es2 at a regular distance of 5 m and at mid-point positions. Considering the length of Es1 (100 m) and Es2 (80 m), 39 and 33 starting points were identified, respectively;

(b) Number of initial velocity (nV_0), corresponding to the number of release points on the cliff, on the vertical line of each starting point: uncertainty in initial velocity was accounted for by considering different detachment elevations (H_i). Each V_{0i} was then calculated in correspondence of the starting line according to:

$$V_{0i} = C_S\sqrt{2gH_i}, \quad (1)$$

where H_i is the elevation difference between the release point i and the starting line, g is the gravity acceleration; C_S is a damping coefficient ($0 < C_S < 1$) that accounts for possible impacts of falling blocks on the rock slope edge.

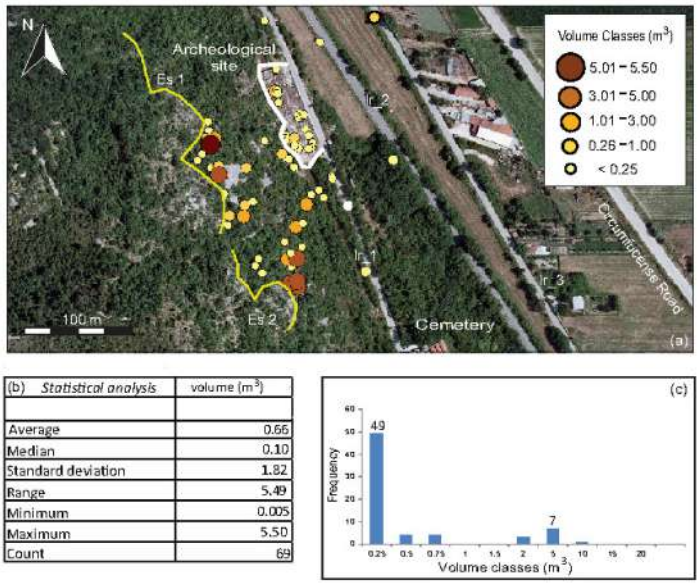

(b) *Statistical analysis*	volume (m³)
Average	0.66
Median	0.10
Standard deviation	1.82
Range	5.49
Minimum	0.005
Maximum	5.50
Count	69

Figure 5. (**a**) Rock block inventory map. Volume classes are reported in the upper right box. Yellow lines represent the traces of the main rock escarpments Es1 and Es2; (**b**) basic statistical analysis; (**c**) frequency histogram.

In this study, three H_i values have been used for Es1 (i.e., 3, 6, and 10 m), and four H_i values for Es2 (i.e., 5, 10, 15, and 20 m). C_S was assumed equal to 1 considering the sub-vertical cliff geometry. For Es1 and Es2, minimum and maximum V_0 values equal to 7.67–14 m/s and 9.90 –19.81 m/s were calculated, respectively;

(c) Number of angular deviations (nA_d) for each detachment point: this number represents the number of allowed initial motion directions out of the maximum slope direction plane. This parameter accounts for the lateral dispersion of the trajectories. Initially, four angular deviations with a maximum angle of 10° for each starting point were assumed, and this choice was confirmed after the model calibration.

Finally, considering all the input parameters for each rock slope escarpment Rotomap® simulated a number of 3-D trajectories (nT) through Equation (2):

$$nT = nS_p \cdot nV_0 \cdot nA_d. \quad (2)$$

A total of 996 rock block trajectories resulted from the numerical simulation, 468 from Es1 and 528 from Es2.

3.2.3. Kinematic Parameters

A slope classification is required to identify terrain classes with different values of kinematic parameters. Normal (K_n) and tangential (K_t) restitution coefficients can be defined according to:

$$K_n = V_n^f / V_n^i, \quad (3)$$

$$K_t = V_t^f / V_t^i, \quad (4)$$

where V^f and V^i are rock block velocities after and before rebounds. These parameters quantify the loss of energy during the impacts and consider the elasto-plastic deformation of the ground surface. K_n and K_t values can vary between 1 (no energy loss during impact, which means perfectly elastic impact) to 0 (i.e., perfectly plastic impact, which causes the block arrest). K_n is conditioned by the material properties and impact condition on the slope surface; for rotating blocks impacting at shallow angles K_n may result >1. Similarly, the dynamic friction angle ($\Phi_{\mu d}$) can vary between 0 and 1, depending on the slope dip angle, the block size, and the ground roughness.

After a detailed geomorphological survey and aerial photographs analysis, six slope classes were defined for the slope overhanging the *Lucus Angitiae* archaeological site (Figure 6). Since in situ rockfall tests are strictly forbidden in the study area, the estimation of the kinematic parameters was made through a detailed literature review (Table 1), which comprises: field tests [24,37–46], back analysis simulations [35,41,47–53] and experimental analogue modeling [54].

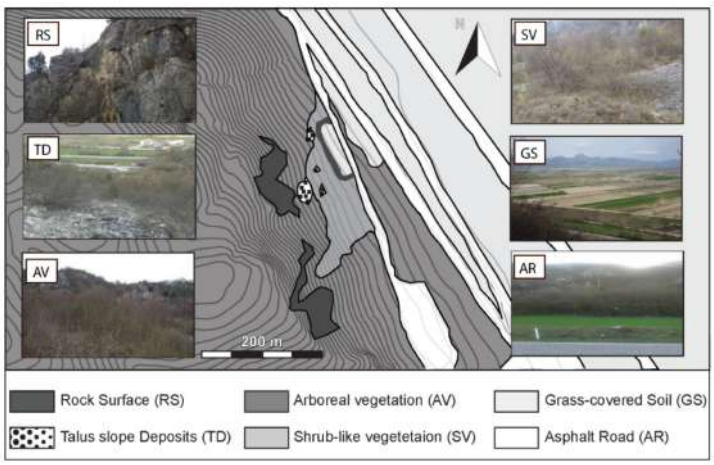

Figure 6. Slope terrain classification.

Table 1. Literature review of kinematic parameters values for slope terrain classes recognized in the study area. Legend: RS = Rock slope; TD = Talus Deposits; AV = Arboreal Vegetation; SV = Shrub-like Vegetation; GS = Grass-covered Soil; AR = Asphalt Road.

	RS			**TD**			**AV**		
	K_n	K_t	$\varphi_{\mu d}$	K_n	K_t	$\varphi_{\mu d}$	K_n	K_t	$\varphi_{\mu d}$
[38]	0.75–0.80 (k)								
[55]	0.65–0.75	0.8–0.9		0.45–0.65	0.5–0.86	0.65			
[56]				0.32	0.8	0.65			
[57]	0.8	0.8							
[47]							0.30–0.33	0.8–0.83	
[40]				0.3–0.33	0.83–0.87				
[58]				0.3			0.25		
[42]	0.2	0.53							
[44]	0.51–0.92 (k)			0.32–0.65(k)					
[45]	0.75–0.90 (k)		0.40–0.45	0.55–0.70 (k)		0.65–0.80			
[43]				0,3	0,61				
[54]	0.4–0.6	0.65–0.9							
[35]				0.35	0.7	0.6	0.35	0.65	0.55
[50]	0.65	0.8	0.3	0.35	0.55	0.7			
[51]	0.65 ± 0.0175	0.75 ± 0.0275	0.25 ± 0.01	0.35 ± 0.0175	0.55 ± 0.0275	0.65 ± 0.03			
[24]	0.6	0.8	0.2	0.4	0.63–1.4	0.65	0.2	0.4	0.7
min/max aver.	0.594–0.765	0.714–0.737	0.287–0.24	0.362–0.397	0.604–0.655	0.65–0.582	0.275–0.282	0.616–0.626	0.625
aver.	0.6795	0.7255	0.527	0.3795	0.6295	0.616	0.278	0.621	0.625
	SV			**GS**			**AR**		
	K_n	K_t	$\varphi_{\mu d}$	K_n	K_t	$\varphi_{\mu d}$	K_n	K_t	$\varphi_{\mu d}$
[38].									
[55]				0.2–0.3	0.2–0.4				
[56]				0.3	0.8		0.4	0.9	0.45
[57]									
[47]	0.30–0.33	0.83–0.87		0.28–0.32	0.68–0.72		0.37–0.42	0.87–0.92	
[40]		0.82–0.85		0.28–0.33			0.37–0.42	0.87–0.92	
[58]									
[42]									
[44]									
[45]				0.50–0.60 (k)		0.45–0.65	0.75(k)		0.40–0.45
[43]									
[54]									
[35]	0.33	0.75	0.5	0.3	0.7	0.6	0.45	0.7	0.6
[50]				0.15	0.2	0.85			
[51]				0.15 ± 0.025	0.3 ± 0.015	0.8 ± 0.04			
[24]				0.4	0.5	0.3	0.4	0.9	0.2
min/max averages	0.315–0.33	0.8–0.823	0.5	0.284–0.302	0.485–0.491	0.6–0.488	0.456–0.473	0.831–0.848	0.413–0.425
averaged	0.3225	0.8115	0.5	0.293	0.488	0.544	0.4645	0.8395	0.419

3.3. Geomechanical and Sensitivity Analyses

Geomechanical analysis was completed at station S_1, in correspondence of the source area of the 2005 rockfall event, along the base of main escarpments Es1 (Figures 3a and 4a). Collected data were used to estimate the size of the missing or potentially detachable rock blocks through the Swedge® software code [59].

In addition, strength parameters along the main discontinuities were evaluated. The residual friction angle (Φ_r) was inferred by applying the relation proposed by [60]:

$$\Phi_r = (\Phi_b - 20) + 20(r/R), \quad (5)$$

where r and R are the Schmidt rebound values measured on weathered and unweathered joint surfaces, respectively. A basic friction angle $\Phi_b = 35^\circ$ for a generic unweathered joint surface in dolomitic limestone was assumed by literature [61–66]. The Joint Roughness Coefficient (JRC) and the Joint wall Compressive Strength (JCS) were also evaluated in-situ for main joint sets. Stability analyses were then completed for rock wedges identified on escarpments Es1, using the Swedge® code and adopting the strength criterion proposed by [67]. Factor of Safety values (FS) were estimated under dry and static conditions.

As a last operation, we performed sensitivity analyses to investigate the role of water pressure and seismic actions as potential triggering factors for rockfall events [68]. As regards the first factor, different authors analyzed the water effect on rockfall/rockslide occurrence, evaluating both critical water heights within upslope tension cracks [69,70] and freeze-thaw episodes in cold areas, where ice which forms within cracks can lead to failure [71–73]. In this study, water pressure (u) variation was simulated through the "Percentage Filled Fissures" option in Swedge®, which allows to specify the average height of water within joint surfaces as a percentage of the completely water-filled state. As regards the seismic action, the sensitivity analysis was performed considering the FS versus the seismic coefficient (a), which defines the seismic acceleration as a fraction of the gravity acceleration. In the performed analyses, the seismic force was applied horizontally, in correspondence of the centroid of the wedges.

3.4. Seismic Action Assessment DEM

According to a newspaper article (Figure 2f), the rockfall in 2005 was caused by heavy rainfall. Nevertheless, the *Lucus Angitiae* archaeological site is located at the western border of the Fucino Basin, which is one of the main seismogenetic area of central Apennines: thus, an assessment of seismic input is advisable.

Since the rockfall process involves rigid bedrock material, the dynamic response of the rock mass can be ignored, and the natural period of the sliding mass (Ts) may be considered essentially zero [74]. This implies that the seismic action can be defined starting from quantities such as the Peak Ground Acceleration (PGA) reference values.

Assessment of seismic action was derived from the results of the PSHA (Probabilistic Seismic Hazard) map of Italy [75]. Specifically, a selection of PGA was carried out using a probabilistic approach for the identification of the maximum reference seismic action for the *Lucus Angitiae* site (lat: 41.971, long: 13.461).

Finally, using the REXEL code [76] a disaggregation analysis was also performed to identify the magnitude (M) and epicentral distance (R) intervals, that provide a major contribution to the seismic input.

4. Results

Given the initial motion conditions and kinematic parameters in Table 1, iterative numerical simulations of rockfalls were performed. For each modeling step, results were compared with the rock blocks inventory map. Trajectories were considered as reliable when more than 60% of inventoried rock blocks (42 out of 69) were included within a 5 m-wide buffer zone around accumulation areas identified by modeling (Figure 7a). Buffering was imposed to account for uncertainty in GPS localization and possible remobilizations of rock blocks along main roads.

Input and calibrated values for kinematic parameters are listed in Table 2. Differences concern the decrease of K_t values for TD and AV (and partly SV) slope classes and an increase of the same parameter for the GS class. The $\Phi_{\mu d}$ changed for the SV slope class only.

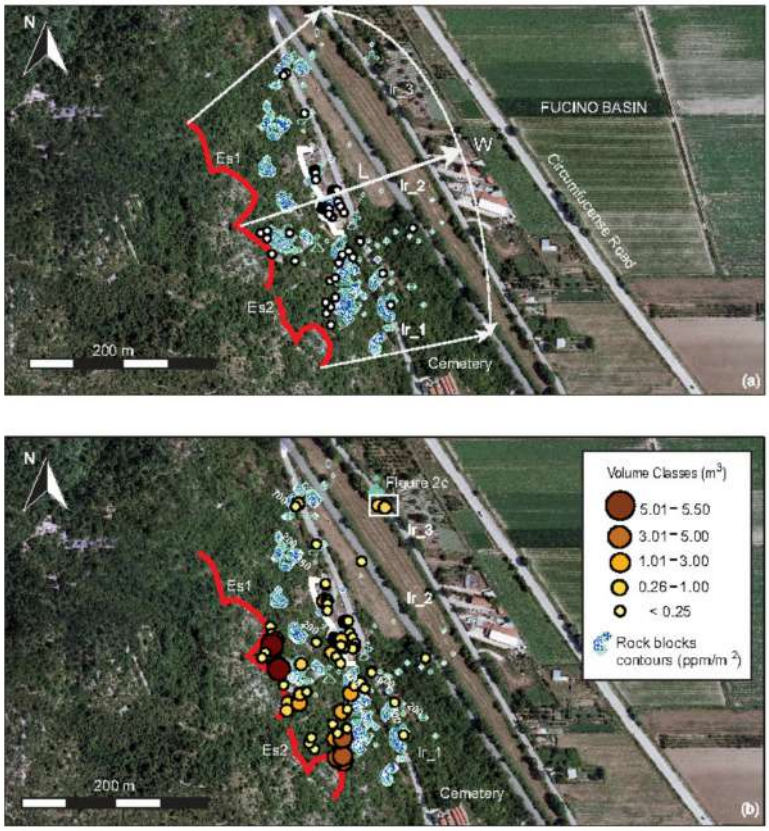

Figure 7. (**a**) Selection of rock blocks falling within a 5 m-buffer distance around arrest points foreseen by the model. Legend: W, L = width and length of accumulation area; (**b**) rock blocks inventory map and arrest points contour lines (expressed as ppm/m^2).

Table 2. Kinematic parameters *Kn*, *Kt* and $\varphi_{\mu d}$ before and after calibration (main variations in italics). Legend: RS = Rock slope; TD = Talus Deposits; AV = Arboreal Vegetation; SV = Shrub-like Vegetation; GS = Grass-covered Soil; AR = Asphalt Road.

(Averaged Values in Table 1)	K_n	K_t	$\varphi_{\mu d}$
RS	0.6795	0.7255	0.527
TD	0.3795	0.6295	0.616
AV	0.278	0.621	0.625
SV	0.3225	0.8115	0.5
GS	0.293	0.488	0.544
AR	0.4645	0.8395	0.419
(values after calibration)	K_n	K_t	$\varphi_{\mu d}$
RS	0.6	0.7	0.45
TD	0.3	*0.3*	0.5
AV	0.3	0.3	0.5
SV	0.5	0.6	*0.8*
GS	0.4	*0.8*	0.5
AR	0.35	0.75	0.6

Figure 7b reports accumulation areas (arrest points) foreseen by the model and the block inventory. The map shows how rock blocks falling from Es1 can reach the archaeological site and local roads lr_1, lr_2 and lr_3. The maximum simulated run-out is compatible

with rock blocks found along the northern tract of lr_3, 230 m far from Es1 (Figure 2c). A lower run-out distance (about 170 m) characterizes rock blocks falling from Es2, which can potentially reach roads lr_1 and lr_2, but not road lr_3.

The W/L ratio of the accumulation area (Figure 7a) is quite low (i.e., 350 m / 230 m = 1.52): such a value is consistent with the simple, biplanar geometry of the Luco dei Marsi dip-slope. Indeed, most of simulated trajectories show slight deviations from the maximum slope direction (Figure 8).

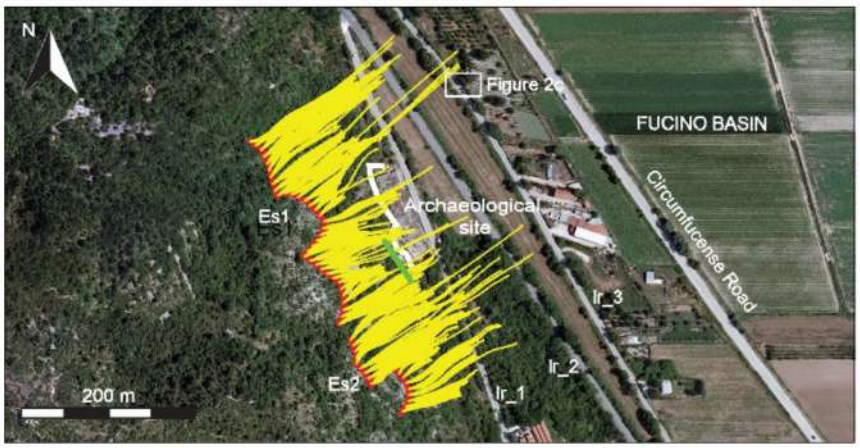

Figure 8. Rock block trajectories map and location of present barrier (thick green line). Position of two blocks shown in Figure 2c is indicated, featuring a 230 m maximum run-out distance.

Figure 9a shows the spatial variation of the specific kinetic energy e_k (m^2/s^2) gained by dimensionless rock blocks falling from Es1. A maximum value of 300 m^2/s^2 is reached in the northern sector of the slope. Around the archaeological site and in correspondence of local roads, e_k varies from 50 to 150 m^2/s^2. A slightly higher maximum value, up to 350 m^2/s^2, characterizes the rock blocks falling from Es2 (Figure 9b), which would reach the local road network (lr_1 and lr_2) with a specific kinetic energy e_k ranging from 50 to 200 m^2/s^2. The last model output is the map of bouncing heights (Figure 10a,b). This map shows that motion along slope basically takes place by rolling with short, few rebounds, which reach maximum heights ranging between 6 and 7 m for Es1 and Es 2. At the western side of the *Lucus Angitiae* archaeological site, bouncing heights is estimated to be 4 m (Figure 10a).

Geomechanical measurements taken at station S_1 are reported in Table 3. Considering the orientation of mechanical discontinuities (including bedding) and the polymetric persistence and spacing of main joint systems, the geometry and volume of the rock block detached in the 2005 rockfall were reconstructed. We assumed a complex wedge resulting from the intersection of bedding (S0), elements of joint sets (J1) acting as tension cracks, and fractures belonging to the other two sets (J2, J3) representing lateral releases (Figure 11a–c). A missing volume of 230 m^3 has been estimated for this detached rock wedge. First-order, wedge-shaped rock pillars having similar dimensions and prone to fall can be observed nearby S_1 (Figures 4a and 11d) and along Es2 (Figure 4b).

Secondary, minor spacing and persistence (both metric-scale) was observed for joint sets J2 and J3 at station S_1. The joints characteristics are uniform along the entire length of Es1 and Es2 and a second-order, missing or prone-to-fall rock blocks were identified and reconstructed (Figure 12a–e). These blocks are characterized by lower volumes, ranging between 2.5 and 5 m^3, and a simpler geometry, which allows the blocks to slide along intersection lines between J2 and J3.

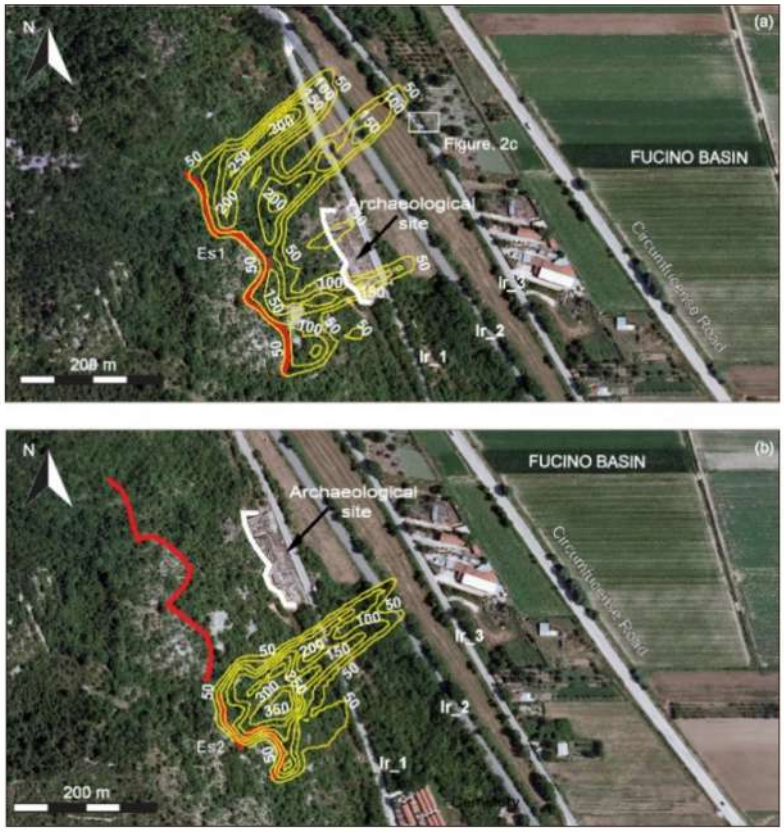

Figure 9. Specific kinetic energies e_k map (m^2/s^2) for rockfall simulations from escarpment: (**a**) Es1; (**b**) Es2.

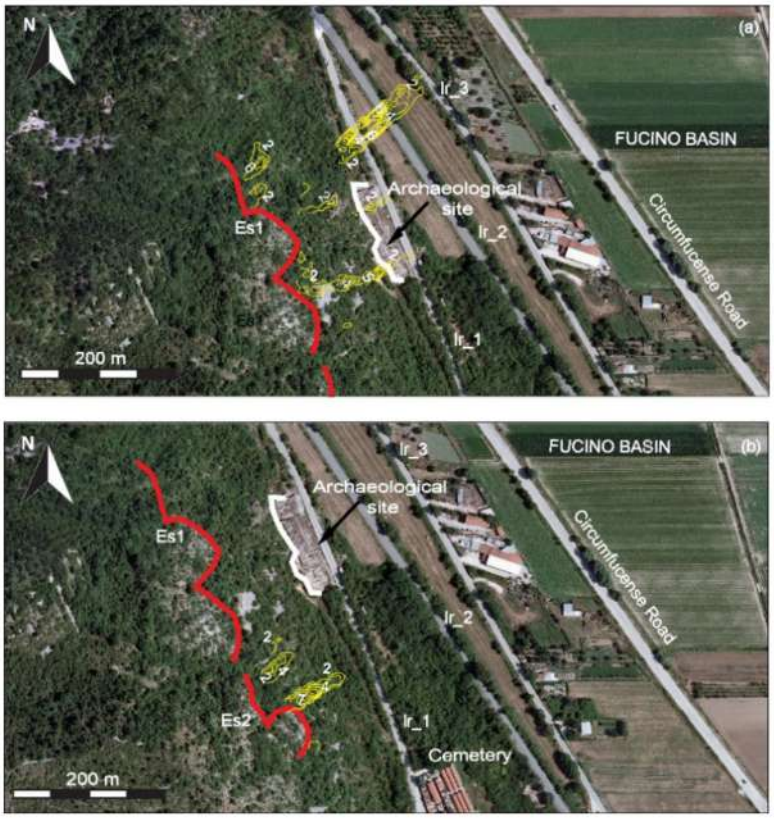

Figure 10. Bouncing heights map (m) for rockfall simulations from escarpment: (**a**) Es1; (**b**) Es2.

Table 3. Geomechanical analysis for main discontinuities at station S_1. Joint data are in Dip/Dip Direction mode. The extreme bounce values of the Schmidt's Hammer, discarded from the calculation of r and R, are reported in italics. Legend: TC = Tension Crack; *Φr* = residual friction angle; JRC = Joint Roughness Coefficient; JCS = Joint Compressive Strength.

S_1	Joint set J1 = TC—Main Plane: 84°;75°	Joint set J2—Main Plane: 170°;77°
R	48,53,52,*54*,50,36,46,40,42,*36*,38,49,48,41	38,32,48,*32*,38,44,32,42,44,48,48,42,*48*
R	54,51,48,55,46,50,*58*,50,48,56,52,*44*, 48,50	53,*58*,44,52,56,40,48,42,56,*42*,44,50,52
Φr	(35–20) + 20(45.25/50.67)=32.86	(35–20) + 20(41.45/48.81)=31.98
JRC	8	10
JCS	80MPa	80 MPa
S_1	Joint set J3—Main Plane: 40°;75°	S0 = 92°;31°
R	44,32,48,38,46,44,34,40,*48*,42,*32*,38,44,40	*32*,44,34,32,44,48,*36*,32,40
R	48,54,*58*,46,54,46,44,*44*,56,58,46,48,50	44,*50*,48,50,44,46,52,48,*44*
Φr	(35–20) + 20(40.83/50.251) = 31.25	(35–20) + 20(38.00/47.33) = 31.05
JRC	10	8
JCS	80MPa	80 MPa

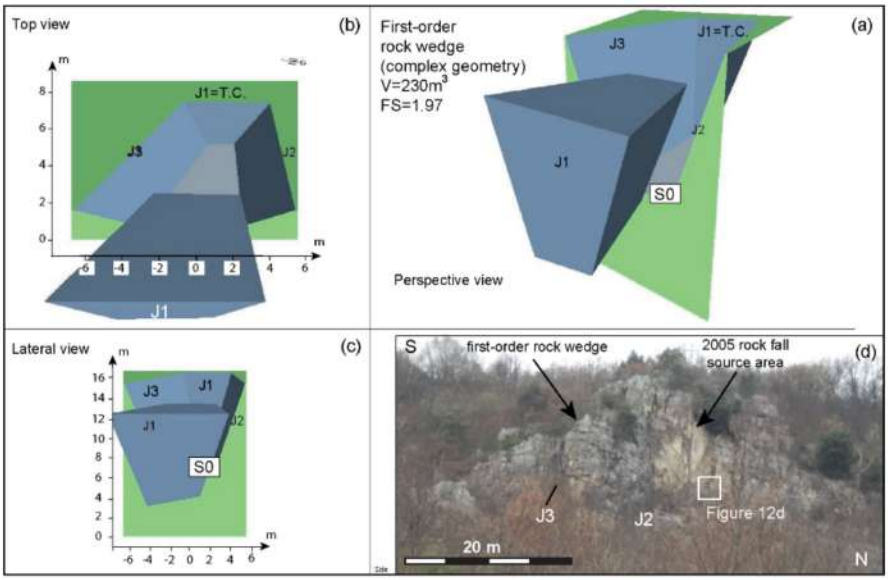

Figure 11. (**a**–**c**) Geometric reconstructions (by Swedge® software) of the first-order rock wedge detached during the 2005 rockfall event; (**d**) rock pillar with similar geometry and size on the Es1 escarpment.

Given the geometry and size of missing—or potentially detachable—rock wedges and considering the strength characteristics of main discontinuity surfaces (Table 3), stability analyses were initially carried out assuming static and dry conditions. A factor of safety (FS) equal to 1.97 has been estimated in a pre-failure condition for the first-order rock wedge detached in the 2005 event (Figure 11a); and an FS equal to 2.86 has been calculated for the second-order rock wedge (Figure 12a).

Results of the sensitivity analyses are reported in Figure 13. Both kinds of rock wedges would reach instability conditions (FS < 1) in response to water pressure resulting from 86% water-filled cracks (Figure 13a,b). Alternatively, if we consider a horizontal seismic force, the seismic input will cause collapse for seismic coefficient equal to a = 0.35 g and a = 0.38 g in the case of first- and second-order rock wedges, respectively (Figure 13c,d).

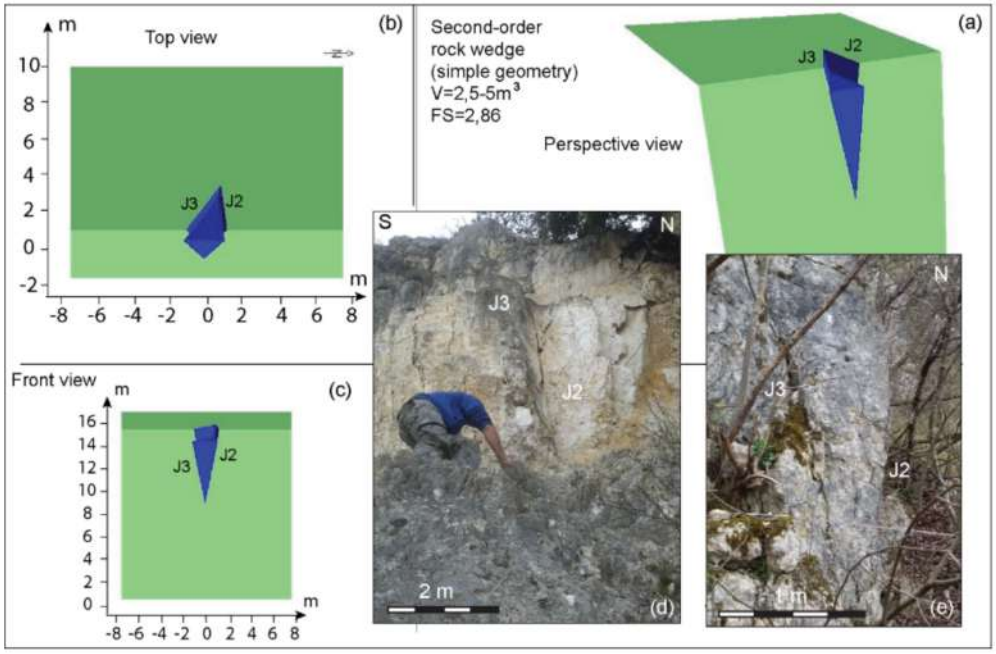

Figure 12. (**a**–**c**) Geometric reconstructions (by Swedge® software) of a missing, second-order rock wedge observed at station St_1; (**d**) the detachment area; (**e**) similar rock wedge geometry observed along Es2.

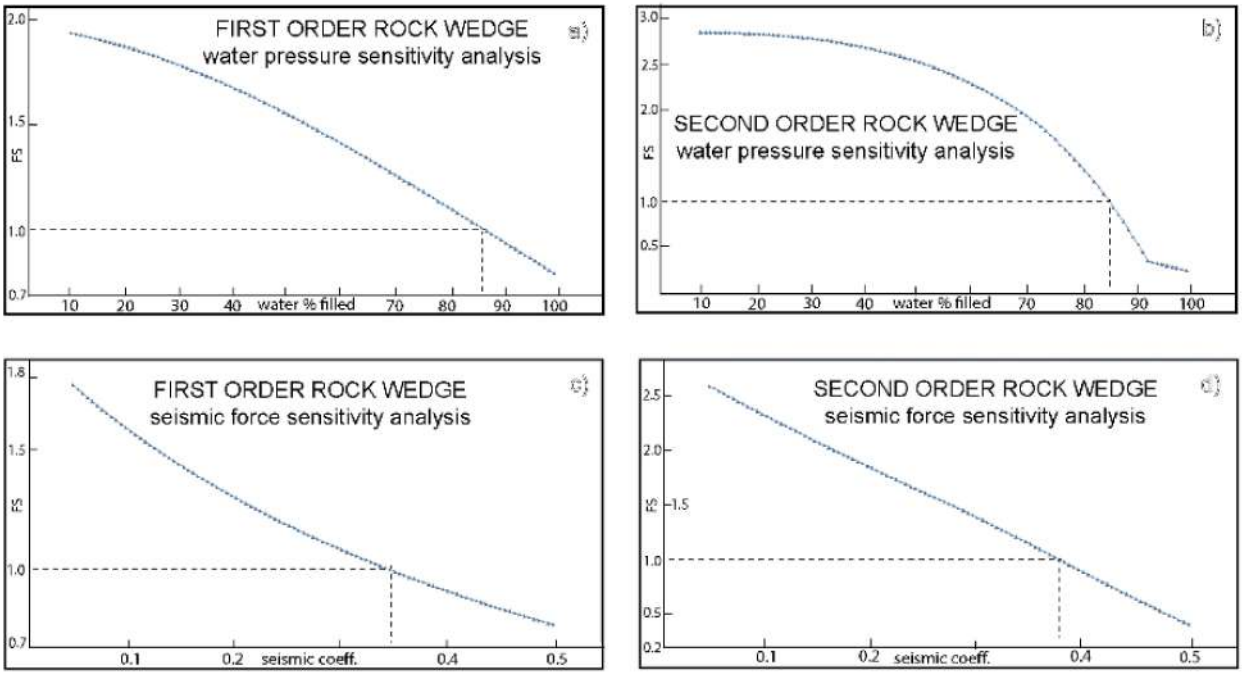

Figure 13. Sensitivity plots: (**a**) FS versus Water Percent Filled for first-order rock wedge; (**b**) FS versus Water Percent Filled for second-order rock wedge; (**c**) FS versus Seismic Coefficient for first-order rock wedge; (**d**) FS versus Seismic Coefficient for second-order rock wedge.

Finally, to estimate the maximum reference seismic action in the area, a probabilistic analysis for the seismic input was carried out. Results are shown in Figure 14a, where the set of PGA values are reported for different annual frequencies of exceedance. PGA values have been derived from the results of the Italian Probabilistic Seismic Hazard map [74]. A PGA value equal to 0.246 g is expected in the area for a return period (T_R) of 475 years

(50th percentile), which represents the typical value employed for the preservation of residential buildings [77]. Nevertheless, the level of protection for this site may be studied assuming higher T_R due to the necessity of avoiding any possible damage or collapse in the longer term, ensuring a proper conservation of the cultural heritage. Thus, an analysis for a T_R of 2475 years (50th percentile) was performed and a PGA value equal to 0.435 g was estimated. A disaggregation analysis was also completed using the REXEL code [75] to assess the magnitude and epicentral distance (R) intervals that give a major contribution to the seismic input. The disaggregation analysis highlights that the seismic hazard is mainly due to events with magnitude ranging from 5.0 end 7 and distances between 0 and 20 km from the archaeological site (Figure 14b, upper panel), although very low-rate events may dominate the seismic hazard level (Figure 14b, lower panel).

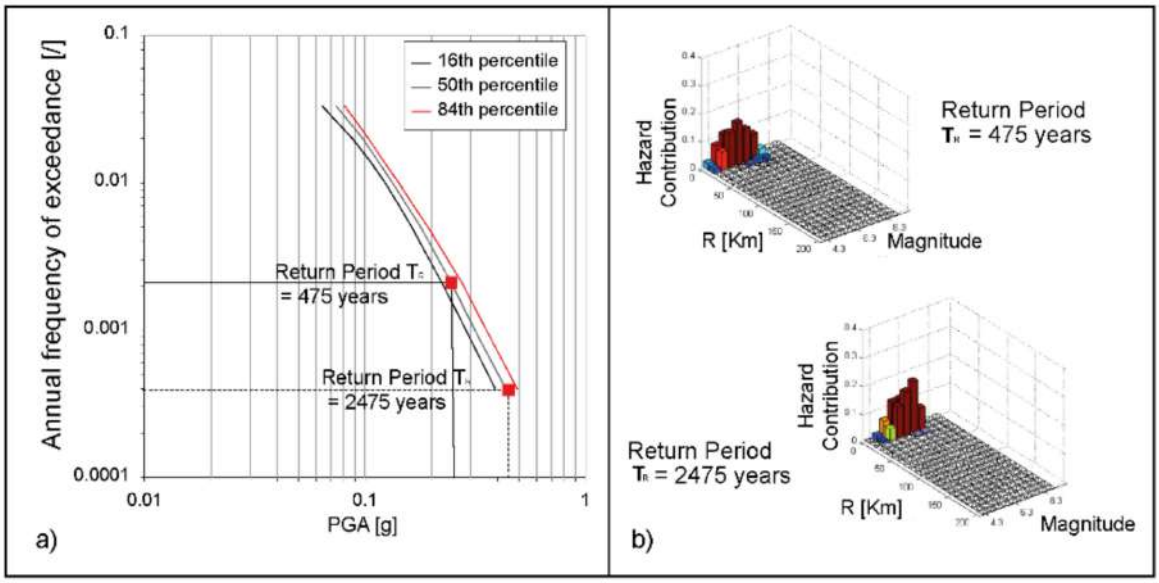

Figure 14. (**a**) PGA as a function of the annual frequencies of exceedance; (**b**) disaggregation analyses for 475. years and 2475 years and for PGA (Ts = 0).

5. Discussion

The potential impact of natural disasters such as extreme meteorological events or strong earthquakes on cultural heritage calls for effective response, deriving from a comprehensive study of the geohazard conditions. In this sense, currently existing protection measures for the *Lucus Angitiae* archaeological site should be replaced or adapted. In fact, the results of the probabilistic modeling indicate that the installed elastic barriers (Figure 1b, Figure 2b, and Figure 2c) may arrest only blocks falling from Es1: specifically, only the southern sector of the archaeological site is currently protected, (Figure 8).

Thus, an updated defensive system was planned by combining the modelled spatial distribution of specific kinetic energies and bouncing heights with the estimated volumes of rock blocks potentially detaching from Es1 and Es2. In this respect, different design blocks (D_b) were considered based upon geomechanical analysis and block dimensioning at stations S_1 and statistical analysis of fallen rock block volumes.

The first design block (D_b1) has a volume of 5 m^3, which is consistent with the maximum dimensions of the observed and reconstructed second-order rock wedges (Figure 12), and the higher mode of rock block frequency distribution (Figure 5c). The second design block (D_b2) has a volume of 2.48 m^3, which was assumed considering the average volume (0.66 m^3) of rock block inventory increased by the standard deviation (1.82 m^3) (Figure 5b). The adopted value is consistent with the minimum size of second-order rock wedges on Es1 and Es2 (i.e., 2.5 m^3). It is important to notice that the most frequent value (0.25 m^3) of block frequency distribution was not considered for design due to the lack of evidence of

small-size rock wedges for both Es1 and Es2. This inconsistency can be explained considering a large fragmentation for both Db1 and Db2 design blocks along trajectories (98% and 90.1%, respectively) (Table 4).

Table 4. Main characteristics of unstable wedges or rock escarpments, design blocks (Db), and protection barriers.

Potentially Unstable Wedges on Es1, Es2	**Second-Order**	**Second-Order**		**First-Order**
Volume (m^3)	5	2.5		230
Design block (Db)	Db1	Db2		Db1
Design block volume (m^3) adopted	5	0.66 + 1.82 = 2.48		5
Fragmentation to 0.25 m^3	95%	90.1%	Frag. from 230 to 5 m^3	97.8%
Design block mass (kg)	12,500	6200		12,500
Design block weight (N)	122,625	60,822		122,625
Barriers				
Specific kinetic energy (m^2/s^2)	200	200		200
Impact energy (kJ)	2500	1240		2500
Energy absorption capacity (kJ)	3000	2000		3000
Height (m)	4	4		4

In this respect, we are aware that a comprehensive mitigation plan should also include rock blocks of greater size, comparable with the missing rock wedge on Es1 (230 m^3) or similar rock pillars outcropping on both Es1 and Es2 (Figure 4a,b and Figure 11d). However, if we observe the rock block inventory in Figure 5a, it can be noticed that only one rock block exceeds the D_b1 volume (i.e., a 5.5 m^3 boulder at the base of Es1), while only few blocks with volumes between 3.01 and 5 m^3 can be found in the uppermost part of the slope. These clues then justify the above-mentioned fragmentation also for very large blocks (97.8% to 5 m^3) which, in turn, can be related to the persistent internal fracturing of rock mass (Table 4). Therefore, the designed block D_b1 can be assumed as representative even of large rockfall events.

In the light of these considerations, a preliminary rockfall mitigation plan was designed. Specifically, we defined the position and size of elastic barriers along the entire perimeter of the archaeological site and the upslope border of local road lr_1 (Figure 15). Along this alignment, the maximum specific kinetic energy e_k is equal to 200 m^2/s^2, which corresponds to different values of impact energy (kJ) as a function of the design block. In the case of D_b1, retaining structures must bear 2500 kJ at the impact and an energy absorption of 3000 kJ is advisable to increase the security level. For the D_b2 block an energy absorption greater than 1240 kJ is required (2000 kJ). In both cases, the barriers should be 4 m high to ensure that rockfalls with all possible trajectories will be contained by the structure. As aforementioned, the 2005 rockfall event was triggered by heavy and prolonged rainfall. This evidence is consistent with the results of the sensitivity analysis for water pressure, since almost the entire length of mechanical discontinuities should be water-filled to induce failures of first and second-order rock wedges (Figure 13a,b). As regards the seismic action (applied along the horizontal direction), the results of the sensitivity analysis reported in Figure 13c,d indicate that the PGA value expected for a return period (T_R) of 475 years (i.e., 0.246 g see Figure 14a), would not cause any rockfall event, being lower than threshold values (i.e., 0.35 and 0.38 g). Only if we consider a larger earthquake (T_R = 2475 years), the corresponding seismic input (i.e., PGA = 0.435 g) could induce rock block failures.

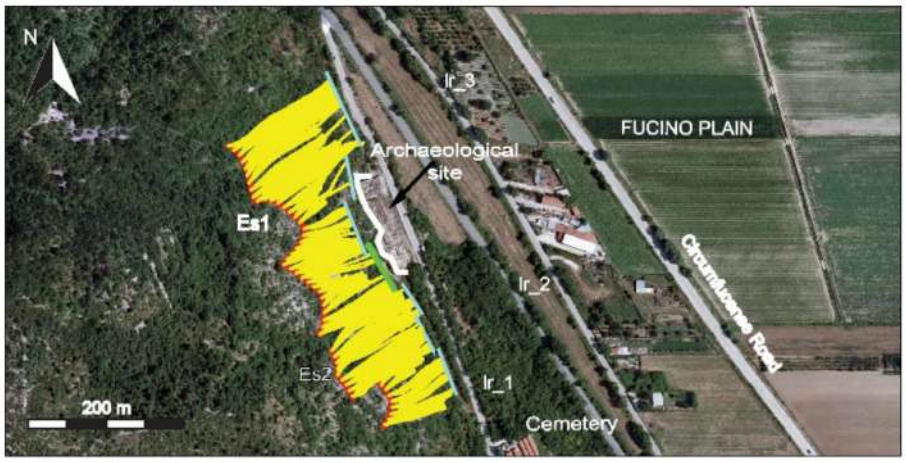

Figure 15. Mitigation measures designed after modelling results which include the installation of further barriers along the slope (thin, light blue lines).

Indeed, the contribution to the seismic hazard shown in Figure 14b is furtherly investigated through the analysis of the historical and instrumental catalogues [34], which show how an intermediate ($4.5 < I_{MCS} < 6$) to damaging ($I_{MCS} > 6$) seismicity is expected for the study area from low distance earthquakes (red box in Figure 16).

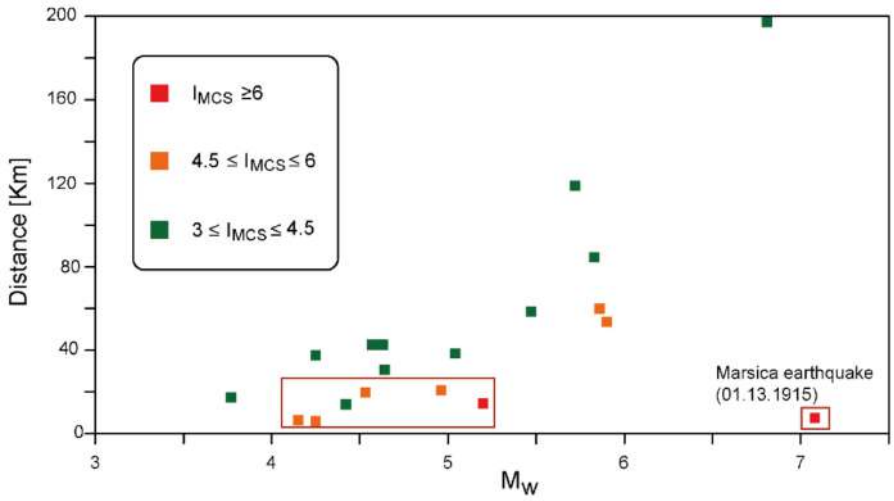

Figure 16. Mw-Distance pairs for events responsible of different macroseismic intensities, I_{MCS}, at the *Lucus Angitiae* site: red squares refer to $I_{MCS} \geq 6$, orange squares refer to $4.5 \leq I_{MCS} < 6$, while green squares to $3 \leq I_{MCS} < 4.5$.

Thus, the safeguard of the *Lucus Angitiae* archaeological site in relation to rockfall hazard should be correctly pursued considering the real extension and magnitude of the rockfall processes. In this sense, further investigations are necessary to evaluate the stability conditions over time of the rock slabs observed along the eastern edge of the slope. In fact, the detachment of very large blocks, with volumes much higher than those estimated in this study for the design blocks, cannot be excluded. These events should be considered as a potential, catastrophic evolution of still unidentified gravity-driven processes acting at the slope scale.

6. Conclusions

In this paper, a 3-D probabilistic model was performed to assess active rockfall processes from a carbonate slope threatening the *Lucus Angitiae* archaeological site in central Italy. Input data were defined based on geomorphological analysis and a critical review

of the scientific literature. Numerical simulations were then performed using as main constraint a comprehensive inventory of blocks identified along the slope. The results emphasize how rockfalls represent a serious hazard not only for the archaeological site but also for the local road network. Therefore, countermeasures such as retaining barriers were designed by dimensioning two different design blocks, in agreement with inventory statistics and evidence from source areas, including the detachment scar of a former rockfall event documented in 2005.

Two different orders of missing or potentially unstable wedge-shaped blocks were recognized on rock escarpments, with volumes ranging from 2.5 to few hundreds of cubic meters. Stability analyses were first performed adopting a simple equilibrium method in dry and static condition. Then, the sensitivity to water pressure variations and seismic inputs was evaluated for both first- and second-order rock wedges. The role of seismic action as triggering factor was acknowledged being the archaeological site located on the border of the main seismogenetic area of central Apennine.

Finally, it can be hypothesized that rockfalls described in this work are only a secondary effect of a slope-scale rock slope deformation, which is driven by the tectonic disarticulation of the carbonate mountain ridge. In this respect, geomorphological evidence of a gravity-driven process is represented by large trench zones delimiting huge rock slabs from which rockfalls can occur.

Author Contributions: Conceptualization, E.D.L.; methodology, E.D.L., L.S. and I.G.; software, E.D.L.; formal analysis, E.D.L.; L.S. and I.G.; field investigation, E.D.L.; data curation, E.D.L., L.S. and I.G.; writing—original draft preparation, E.D.L., L.S. and I.G.; writing—review and editing, E.D.L., L.S. and I.G.; supervision, E.D.L. All authors have read and agreed to the published version of the manuscript.

Funding: This research received no external funding.

Data Availability Statement: I exclude this statement since the study did not report any data.

Acknowledgments: This work was completed in the frame of the "Master in Analysis and Mitigation of Hydrogeological Risk" organized by "Sapienza" University of Rome. Authors are grateful to Francesca Bozzano and Ilaria Fiori who helped in field surveys and initial modelling.

Conflicts of Interest: The authors declare no conflict of interest.

References

1. Nicu, I.C. Natural hazards-a threat for immovable cultural heritage, A review. *Int. J. Conserv. Sci.* **2017**, *8*, 375–388.
2. Klimeš, J. Landslide temporal analysis and susceptibility assessment as bases for landslide mitigation, Machu Picchu, Peru. *Environ. Earth Sci.* **2013**, *70*, 913–925. [CrossRef]
3. Schilirò, L.; Cevasco, A.; Esposito, C.; Mugnozza, G.S. Shallow landslide initiation on terraced slopes: Inferences from a physically based approach. *Geomat. Nat. Hazards Risk* **2018**, *9*, 295–324. [CrossRef]
4. Tunusluoglu, M.C.; Zorlu, K. Rockfall hazard assessment in a cultural and natural heritage (Ortahisar Castle, Cappadocia, Turkey). *Environ. Geol.* **2009**, *56*, 963–972. [CrossRef]
5. Marchetti, D.; Avanzi, G.A.; Sciarra, N.; Calista, M.; Mazzanti, G. Numerical Modeling Applied to a Cultural Heritage Site Threatened by Rock Falls in Tuscany (Italy). In *Rock Mechanics in Civil and Environmental Engineering*; Zhao, L., Dudt, M., Eds.; Taylor & Francis Group: London, UK, 2010; pp. 647–650.
6. Di Luzio, E.; Fasani, G.B.; Bretschneider, A. Potential rockfalls and analysis of slope dynamics in the Palatine archaeological area. *Geol. Acta* **2013**, *11*, 245–264. [CrossRef]
7. Di Luzio, E.; Colosi, F.; Fidenzi, E.; Malinverni, E.S.; Gaudiosi, I.; Bozzi, C.A.; Orazi, R. Slope analysis and rock fall assessment in the Khinis archaeological area (Kurdistan, northern Iraq). *Ital. J. Eng. Geol. Environ.* **2019**, *19*, 13–35. [CrossRef]
8. Wang, X.; Zhang, L.; Wang, S.; Agliardi, F.; Frattini, P.; Crosta, G.B.; Yang, Z. Field investigation and rockfall hazard zonation at the Shijing Mountains Sutra caves cultural heritage (China). *Environ. Earth Sci.* **2012**, *66*, 1897–1908. [CrossRef]
9. Di Luzio, E.; Mazzanti, P.; Brunetti, A.; Baleani, M. Assessment of tectonic-controlled rock fall processes threatening the ancient Appia route at the Aurunci Mountain pass (central Italy). *Nat. Hazards* **2020**, *102*, 909–938. [CrossRef]
10. Dinçer, I.; Orhan, A.; Frattini, P.; Crosta, G.B. Rockfall at the heritage site of the Tatlarin Underground City (Cappadocia, Turkey). *Nat. Hazards* **2016**, *82*, 1075–1098. [CrossRef]
11. Fanti, R.; Gigli, G.; Lombardi, L.; Tapete, D.; Canuti, P. Terrestrial laser scanning for rock fall stability analysis in the cultural heritage site of Pitigliano (Italy). *Landslides* **2013**, *10*, 409–420. [CrossRef]

12. Margottini, C.; Antidze, N.; Corominas, J.; Crosta, G.B.; Frattini, P.; Gigli, G.; Giordan, D.; Iwasaky, I.; Lollino, G.; Manconi, A.; et al. Landslide hazard, monitoring and conservation strategy for the safeguard of Vardzia Byzantine monastery complex, Georgia. *Landslides* **2015**, *12*, 193–204. [CrossRef]
13. Boldini, D.; Guido, G.L.; Margottini, C.; Spizzichino, D. Stability analysis of a large-volume block in the historical rock-cut city of Vardzia (Georgia). *Rock Mech. Rock Eng.* **2018**, *51*, 341–349. [CrossRef]
14. Frodella, W.; Elashvili, M.; Spizzichino, D.; Gigli, G.; Nadaraia, A.; Kirkitadze, G.; Adikashvili, L.; Margottini, C.; Antidze, N.; Casagli, N. Applying Close Range Non-Destructive Techniques for the Detection of Conservation Problems in Rock-Carved Cultural Heritage Sites. *Remote Sens.* **2021**, *13*, 1040. [CrossRef]
15. Tarragüel, A.A.; Krol, B.; van Westen, C. Analysing the possible impact of landslides and avalanches on cultural heritage in Upper Svaneti, Georgia. *J. Cult. Herit.* **2012**, *13*, 453–461. [CrossRef]
16. Michalski, S.; Pedersoli, J.L., Jr. The ABC Method: A Risk Management Approach to the Preservation of Cultural Heritage. Available online: https://www.iccrom.org/it/publication/abc-method-risk-management-approach-preservation-cultural-heritage (accessed on 15 November 2021).
17. Valagussa, A.; Frattini, P.; Crosta, G.; Spizzichino, D.; Leoni, G.; Margottini, C. Multi-risk analysis on European cultural and natural UNESCO heritage sites. *Nat. Hazards* **2021**, *105*, 2659–2676. [CrossRef]
18. Monaghan, P. *Encyclopedia of Goddess and Heroines*; Greenwood Press: Santa Barbara, CA, USA, 2009; p. 641.
19. Galadini, F.; Ceccaroni, E.; Falcucci, E.; Gori, S. Natural hazards in the Abruzzi Apennines (Italy) and the risk to archaeological sites. *Disaster Adv.* **2012**, *5*, 72–78.
20. Scioldo, G. Rotomap: Analisi Statistica del Rotolamento dei Massi. In *Guida di Informatica Ambientale*; Guariso, G., Ed.; Patron: Bologna, Italy, 1991; pp. 81–84.
21. Geo&Soft International, RotoMap 32. Available online: https://www.geoandsoft.com/italiano/geomeccanica_software_calcolo_caduta_rotolamento_massi.htm (accessed on 10 December 2021). CNR License number T3N2781(16-18-34).
22. Del Maschio, L.; Gozza, G.; Piacentini, D.; Pizziolo, M.; Soldati, M. Previsione delle traiettorie dei blocchi mobilizzati da frane di crollo: Applicazione e confronto di modelli. *G. Geol. Appl.* **2007**, *6*, 33–44.
23. Bourrier, F.; Dorren, L.; Nicot, F.; Berger, F.; Darve, F. Toward objective rockfall trajectory simulation using a stochastic impact model. *Geomorphology* **2009**, *110*, 68–79. [CrossRef]
24. Ferrari, F.; Giani, G.P.; Apuani, T. Towards the comprehension of rockfall motion, with the aid of in situ tests. *Ital. J. Eng. Geol. Environ.* **2013**, *6*, 163–171. [CrossRef]
25. Patacca, E.; Scandone, P.; Di Luzio, E.; Cavinato, G.P.; Parotto, M. Structural architecture of the central Apennines: Interpretation of the CROP 11 seismic profile from the Adriatic coast to the orographic divide. *Tectonics* **2008**, *27*. [CrossRef]
26. Cosentino, D.; Cipollari, P.; Marsili, P.; Scrocca, D. Geology of the Central Apennines: A Regional Review, The Geology of Italy: Tectonics and Life along Plate Margins. *J. Virtual Explor.* **2010**, *12*. [CrossRef]
27. Galadini, F.; Messina, P. Plio-Quaternary tectonics of the Fucino basin and surrounding areas (central Italy). *G. Geol.* **1994**, *56*, 73–99.
28. Bosi, C.; Galadini, F.; Messina, P. Stratigrafia plio-pleistocenica della Conca del Fucino. *Quaternario* **1995**, *8*, 83–94.
29. Cavinato, G.P.; Carusi, C.; Dall'Asta, M.; Miccadei, E.; Piacentini, T. Sedimentary and tectonic evolution of Plio-Pleistocene alluvial and lacustrine deposits of Fucino Basin (central Italy). *Sediment. Geol.* **2002**, *148*, 29–59. [CrossRef]
30. Galadini, F.; Messina, P.; Giaccio, B.; Sposato, A. Early uplift history of the Abruzzi Apennines (central Italy): Available geomorphological constraints. *Quat. Int.* **2003**, *101-102*, 125–135. [CrossRef]
31. Michetti, A.M.; Brunamonte, F.; Serva, L.; Vittori, E. Trench investigations of the 1915 Fucino earthquake fault scarps (Abruzzo, Central Italy): Geological evidence of large historical events. *J. Geophys. Res. Solid Earth* **1996**, *101*, 5921–5936. [CrossRef]
32. Galadini, F.; Galli, P. The Holocene paleoearthquakes on the 1915 Avezzano earthquake faults (central Italy): Implications for active tectonics in the central Apennines. *Tectonophysics* **2000**, *308*, 143–170. [CrossRef]
33. Galadini, F.; Galli, P. Active tectonics in the Central Apennines (Italy). Input data for seismic hazard assessment. *Nat. Hazards* **2000**, *22*, 225–268. [CrossRef]
34. Rovida, A.; Locati, M.; Camassi, R.; Lolli, B.; Gasperini, P.; Antonucci, A. *Catalogo Parametrico dei Terremoti Italiani (CPTI15), Versione 3.0*; Istituto Nazionale di Geofisica e Vulcanologia (INGV): Rome, Italy, 2021. [CrossRef]
35. Agliardi, F.; Crosta, G.B. High resolution three-dimensional numerical modelling of rockfalls. *Int. J. Rock Mech. Min. Sci.* **2003**, *40*, 455–471. [CrossRef]
36. Crosta, G.B.; Agliardi, F. Parametric evaluation of 3D dispersion of rockfall trajectories. *Nat. Hazards Earth Syst. Sci.* **2004**, *4*, 583–598. [CrossRef]
37. Ritchie, A.M. Evaluation of rockfall and its control. *Highw. Res. Rec.* **1963**, *17*, 13–28.
38. Broili, L. In situ tests for the study of rockfall. *Geol. Appl. Idrogeol.* **1973**, *8*, 105–111.
39. Wu, S.S. Rockfall evaluation by computer simulation. *Transp. Res. Rec.* **1985**, *1031*, 1–5.
40. Pfeiffer, T.J.; Higgins, J.D. Rockfall hazard analysis using the Colorado rockfall simulation program. *Transp. Res. Rec.* **1990**, *1288*, 117–126.
41. Evans, S.G.; Hungr, O. The assessment of rockfall hazard at the base of talus slopes. *Can. Geotech. J.* **1993**, *30*, 620–636. [CrossRef]
42. Budetta, P.; Santo, A. Morphostructural evolution and related kinematics of rockfalls in Campania (southern Italy): A case study. *Eng. Geol.* **1994**, *36*, 197–210. [CrossRef]

43. Robotham, E.; Wang, M.; Walton, G. Assessment of risk of rockfall from active and abandoned quarry slopes. *Trans. Inst. Min. Metall. Sect. A* **1995**, *104*, 25–33.
44. Azzoni, A.; De Freitas, M.H. Experimentally gained parameters, decisive for rock fall analysis. *Rock Mech. Rock Eng.* **1995**, *28*, 111–124. [CrossRef]
45. Azzoni, A.; La Barbera, G.; Zaninetti, A. Analysis and prediction of rockfalls using a mathematical model. *Int. J. Rock Mech. Min. Sci.* **1995**, *32*, 709–724. [CrossRef]
46. Giani, G.P.; Giacomini, A.; Migliazza, M.; Segalini, A. Experimental and theoretical studies to improve rock fall analysis and protection work design. *Rock Mech. Rock Eng.* **2004**, *37*, 369–389. [CrossRef]
47. Pfeiffer, T.J.; Bowen, T.D. Computer simulation of rockfalls. *Bull. Assoc. Eng. Geol.* **1989**, *26*, 135–146. [CrossRef]
48. Fornaro, M.; Nebbia, M.; Peila, D. Block Falls on Rock Slopes: Application of a Numerical Simulation Program to Some Real Cases. In Proceedings of the 6th International Congress of the IAEG, Amsterdam, The Netherlands, 6–10 August 1990; Price, D.G., Ed.; Amsterdam Balkema: Rotterdam, The Netherlands, 1990; pp. 2173–2180.
49. Kobayashi, Y.; Harp, E.L.; Kagawa, T. Simulation of rockfalls triggered by earthquakes. *Rock Mech. Rock Eng.* **1990**, *23*, 1–20. [CrossRef]
50. Guzzetti, F.; Reichenbach, P.; Wieczorek, G.F. Rockfall hazard and risk assessment in the Yosemite Valley, California, USA. *Nat. Hazards Earth Syst. Sci.* **2003**, *3*, 491–503. [CrossRef]
51. Guzzetti, F.; Reichenbach, P.; Ghigi, S. Rockfall hazard and risk assessment along a transportation corridor in the Nera Valley, Central Italy. *Environ. Manag.* **2004**, *34*, 191–208. [CrossRef]
52. Longo, S.; Oreste, P. Ceppo Morelli block-falls probability study to support the decision of excavating a by-pass tunnel. *Am. J. Eng. Appl. Sci.* **2010**, *3*, 723–727. [CrossRef]
53. Wang, X.; Frattini, P.; Crosta, G.B.; Zhang, L.; Agliardi, F.; Lari, S.; Yang, Z. Uncertainty assessment in quantitative rockfall risk assessment. *Landslides* **2014**, *11*, 711–722. [CrossRef]
54. Chau, K.T.; Wong, R.H.C.; Wu, J.J. Coefficient of restitution and rotational motions of rockfall impacts. *Int. J. Rock Mech. Min. Sci.* **2002**, *39*, 69–77. [CrossRef]
55. Piteau, D.R.; Clayton, R. Computer Rockfall Model. In Proceedings of the Meeting on Rockfall Dynamics and Protective Works Effectiveness, Bergamo, Italy, 20—21 May 1976; pp. 123–125.
56. Hoek, E. *Rockfall: A Computer Program for Predicting Rockfall Trajectories*; Unpublished internal notes; Golder Associates: Vancouver, BC, Canada, 1986.
57. Descoeudres, F.; Zimmermann, T. Three-dimensional dynamic calculation of rockfalls. In Proceedings of the 6th International Society for Rock Mechanics Congress, Montreal, QC, Canada, 30 August–3 September 1987; pp. 337–342.
58. Giani, G.P. *Rock Slope Stability Analysis*; Balkema: Rotterdam, The Netherlands, 1992; p. 374.
59. Rocscience. Swedge 6.0. Available online: https://www.rocscience.com/software/swedge (accessed on 10 December 2021). CNR License number 18324-001.
60. Barton, N.; Choubey, V. The shear strength of rock joints in theory and practice. *Rock Mech.* **1977**, *10*, 1–54. [CrossRef]
61. Hoek, E.; Bray, J.W. *Rock Slope Engineering, Revised*, 3rd ed.; The Institution of Mining and Metallurgy: London, UK, 1981; pp. 341–351.
62. Cruden, D.M.; Hu, X.Q. Basic friction angles of carbonate rocks from Kananaskis country. *Can. Bull. Int. Assoc. Eng. Geol.* **1988**, *38*, 55–59. [CrossRef]
63. Bruce, I.G.; Cruden, D.M.; Eaton, T.M. Use of a tilting table to determine the basic friction angle of hard rock samples. *Can. Geotech. J.* **1989**, *26*, 474–479. [CrossRef]
64. Goodman, R.E. *Introduction to Rock Mechanics*, 2nd ed.; Wiley J and Sons: New York, NY, USA, 1989; p. 576.
65. Gonzalez de Vallejo, L.I.; Ferrer, M.; Ortuno, L.; Oteo, C. *Geoingegneria*; Pearson Education: Milan, Italy, 2005; p. 816.
66. Waltham, A.C. *Foundations of Engineering Geology*, 3rd ed.; Spon Press, Taylor and Francis: London, UK, 2009; p. 104.
67. Barton, N.; Bandis, S. Review of Predictive Capabilities of JRC-JCS Model in Engineering Practice. In Proceedings of the Regional Conference of the International Society for Rock Mechanics, Loen, Norway, 4–6 June 1990; Barton, N., Stephansson, O., Eds.; CRC Press: Boca Raton, FL, USA, 1990; pp. 603–610.
68. Mazzanti, P.; Schilirò, L.; Martino, S.; Antonielli, B.; Brizi, E.; Brunetti, A.; Margottini, C.; Scarascia Mugnozza, G. The Contribution of Terrestrial Laser Scanning to the Analysis of Cliff Slope Stability in Sugano (Central Italy). *Remote Sens.* **2018**, *10*, 1475. [CrossRef]
69. Zhang, S.; Xu, Q.; Peng, D.; Zhu, Z.; Li, W.; Wong, H.; Shen, P. Stability analysis of rock wedge slide subjected to groundwater dynamic evolution. *Eng. Geol.* **2020**, *270*, 105528. [CrossRef]
70. He, K.; Li, Y.; Ma, G.; Hu, X.; Liu, B.; Ma, Z.; Xu, Z. Failure mode analysis of post-seismic rockfall in shattered mountains exemplified by detailed investigation and numerical modelling. *Landslides* **2021**, *18*, 425–446. [CrossRef]
71. Mateos, R.M.; Garcia-Moreno, I.; Azanon, J.M. Freeze-thaw cycles and rainfall as triggering factors of mass movements in a warm Mediterranean region: The case of the Tramuntana Range (Majorca, Spain). *Landslides* **2012**, *9*, 417–432. [CrossRef]
72. Delonca, A.; Gunzburger, Y.; Verdel, T. Statistical correlation between meteorological and rockfall databases. *Nat. Hazards Earth Syst. Sci.* **2014**, *14*, 1953–1964. [CrossRef]
73. D'Amato, J.; Hantz, D.; Guerin, A.; Jaboyedoff, M.; Baillet, L.; Mariscal, A. Influence of meteorological factors on rockfall occurrence in a middle mountain limestone cliff. *Nat. Hazards Earth Syst. Sci.* **2016**, *16*, 719–735. [CrossRef]

74. Jibson, R.W.; Jibson, M.W. *Java Programs for Using Newmark's Method and Simplified Decoupled Analysis to Model Slope Performance During Earthquakes, version 1.1*; U.S. Geological Survey: Reston, VA, USA, 2003.
75. Stucchi, M.; Meletti, C.; Montaldo, V.; Crowley, H.; Calvi, G.M.; Boschi, E. Seismic Hazard Assessment (2003-2009) for the Italian Building Code. *Bull. Seismol. Soc. Am.* **2011**, *101*, 1885–1911. [CrossRef]
76. Iervolino, I.; Galasso, C.; Cosenza, E. REXEL: Computer aided record selection for code-based seismic structural analysis. *Bull. Earthq. Eng.* **2009**, *8*, 339–362. [CrossRef]
77. *CEN-Comité Européen de Normalisaton; 2004: Eurocode 8-EN 1998-1*; General Rules, Seismic Actions and Rules for Buildings; European Committee for Standardization: Bruxelles, Belgium, 2004.